Journal of Drug Delivery Science and Technology 73 (2022) 103455

Contents lists available at ScienceDirect

Journal of Drug Delivery Science and Technology

journal homepage: www.elsevier.com/locate/jddst

Enhancing the anti-psoriatic activity of vitamin D3 employing nanostructured archaeolipid carriers

Yamila Roxana Simioni [a], Noelia Soledad Perez [a], Leandro R.S. Barbosa [b,c], Ana Paula Perez [a], Priscila Schilrreff [a,d], Eder Lilia Romero [a], Maria Jose Morilla [a,*]

[a] Nanomedicine Research and Development Center, Science and Technology Department, National University of Quilmes, Roque Saenz Peña 352, Bernal, B1876BXD, Argentina
[b] Brazilian Synchrotron Light Laboratory (LNLS), Brazilian Center for Research in Energy and Materials (CNPEM), Campinas, SP, 13083-100, Brazil
[c] Institute of Physics, University of São Paulo, São Paulo, SP, 05508-090, Brazil
[d] Institute of Experimental Physics, Freie Universität Berlin, Arnimallee 14, 14195, Berlin, Germany

ARTICLE INFO

Keywords:
Bacterioruberin
Staphylococcus aureus
Anti-inflammatory

ABSTRACT

Psoriasis (Ps) is a multifactorial autoimmune skin disease, where oxidative stress plays a key role in promoting a vicious producing cycle between keratinocytes and immune cells. Vitamin D3 (VD3) regulates the differentiation, apoptosis, and proliferation of keratinocytes, also displaying antioxidant and anti-inflammatory activities. Previous attempts of using topical VD3 as anti-psoriatic agent, failed because of its poor solubility, high hydrophobicity, structural lability, and low bioavailability. Specifically tailored nanoparticles for topical co-delivery of VD3 and antioxidants to activated keratinocytes and macrophages could make Ps treatments more efficient. In this work, structural features, and *in vitro* activity of nanostructured archaeolipid carriers (NAC) containing VD3 plus the antioxidant C50 dipolar carotenoid bacterioruberin (BR) (NAC-VD3), are presented. Ultra-small (70 nm), −39 mV ζ potential, ~5 mg VD3/ml, 0.35 BR μg/ml NAC-VD3, with good storage stability (at least 6 month) consisted of a compritol and BR core, covered by a shell of *sn* 2,3 ether linked archaeolipids and Tween 80 (2: 2: 1.2: 3% w/w) were obtained. Raman, DSC and SAXS analysis showed that VD3 was trapped within the disordered compritol-BR core, impairing its fast release, and protecting VD3 against thermal degradation. NAC-VD3 were extensively captured and displayed high anti-proliferative (65%), anti-inflammatory (IL-8 release) and antioxidant activities (ROS reduction) on a psoriatic model made of $CaCl_2$ differentiated-imiquimod stimulated HaCaT cells, and on lipopolysaccharide induced THP-1 macrophages. Interestingly, the BR extract alone displayed high anti-*Staphylococcus aureus* activity including *anti*-biofilm formation. Overall, the results suggest that NAC-VD3 protect the labile structure of VD3, while enhancing its anti-psoriatic activity and deserves further *in vivo* exploration.

1. Introduction

Development of chronic inflammatory skin diseases, such as psoriasis (Ps) and atopic dermatitis, is mediated by an imbalance between anti- and pro-inflammatory signals. Ps is a multifactorial autoimmune skin disease, that affects 2–5% of the world population, where keratinocytes and immune cells form a vicious psoriasis-producing cycle [1]. Epidermal hyperproliferation (10 folds faster skin turnover) [2], leukocyte infiltration [3] and vascular proliferation in the papillary dermis are main clinical feature of Ps. Generally associated with arthritis, depression and cardiometabolic syndrome [4], Ps negatively affects patient's life quality, requiring long-term treatment, and decreasing life expectancy [5].

Oxidative stress is involved in the activation of relevant signalling pathways of inflammation, including NF-κB, MAPK, which together with the IL-17/IL-23 pathway [6,7] are responsible for the development and persistence of psoriatic lesions. Activated Th1 and Th17 cells and keratinocytes complete the picture of key immune actors in Ps [8,9]. Healthy keratinocytes produce inhibitory cytokines, that allow the skin to remain inflammatory quiescent [10]. In Ps instead, activated

* Corresponding author. Nanomedicine Research & Development Center, Departamento de Ciencia y Tecnología, Universidad Nacional de Quilmes. Roque Saenz Peña 352, Bernal, B1876 BXD, Argentina.
E-mail address: jmorilla@unq.edu.ar (M.J. Morilla).

https://doi.org/10.1016/j.jddst.2022.103455
Received 15 February 2022; Received in revised form 11 April 2022; Accepted 21 May 2022
Available online 24 May 2022
1773-2247/

keratinocytes act as antigen-presenting cells, initiating, or enhancing the activity of immune cells by expressing HLA antigens [11]. Activated keratinocytes also express toll-like receptors (TLRs) and produce cytokines and chemokines that attract monocytes and Th1 cells, Langerhans cells, dendritic cells (DC), and CLA+ (cutaneous lymphocyte antigen) T cells. In particular IL-8, a potent chemokine, accelerates angiogenesis, inflammation, and further keratinocyte proliferation in the psoriatic lesions. Keratinocytes and neutrophils express surface IL-8 receptors, being IL-8 responsible for the accumulation of intraepidermal neutrophils related to inflammatory and treatment-resistant Ps [12].

Currently, there is no complete and satisfactory cure for Ps. Numerous therapies including topical drugs, phototherapy, systemic drugs, and biologics, only alleviate the disease symptoms [13]. Oral-systemic immunosuppressive and anti-inflammatory drugs are used against severe Ps. Biologicals, such as TNF-α inhibitors, have replaced immunosuppressants as the primary systemic therapy for severe Ps and psoriatic arthritis [14]. However, lack of long-term efficacy, regression of Ps upon removal of treatments, prohibitive cost, increased risks of opportunistic infections, autoimmunity, and infusion reactions, limit the use of biologicals [15–17].

Mild Ps suffered by 70% of patients on the other hand, is treated by topical route. Topical treatments include dithranol, calcineurin inhibitors, retinoids, coal tar, dithranol, corticosteroids, emollients, and vitamin D (VD) analogues [18]. VD3 and its analogues regulate differentiation, apoptosis, and proliferation of keratinocytes, regulate immune system damping down inflammation and oxidative stress [5, 19–21]. Such effects are mediated by the nuclear receptors for VD3 on keratinocytes, fibroblasts and plasmacytoid DCs and by an autonomous VD3 pathway in which VD3 is converted to calcitriol, the hormonally active form of VD3. Unfortunately, the use of VD3 is hampered by its poor solubility, high hydrophobicity, and sensitivity to environmental factors such as heat, light, and oxygen [22]. Moreover, the thickened and inflamed *stratum corneum* of psoriatic patients limits the activity of drugs formulated in gels, ointments, or creams [23].

Specifically tailored nanoparticles (Nps) could overcome the limitations of conventional topical dosage forms, providing structural protection to loaded drugs and enhancing drug penetration across the hyperproliferative crusty *stratum corneum* to the viable epidermis. Additionally, topical drug delivery may avoid systemic absorption, contributing to reduce potential adverse systemic effects and enabling the synchronic delivery of two or more drugs [24]. Nanostructured lipid carriers (NLC) made of solid and liquid lipids covered by surfactants and co-surfactant, are biocompatible and biodegradable Np, used to load hydrophobic drugs with high efficiency, protect them from degradation, and keeping them in stable suspension [25,26]. Some works have reported the use of topically applied NLC as carriers for anti-psoriatic drugs [27], where NLC could form a deposit from where drugs could be release or could bypass the *stratum corneum* to reach their cellular targets.

Previously, our group reported the properties of a new type of NLC, named nanostructured archaeolipid carriers (NAC), consisting of compritol and bacterioruberin (BR) core covered by a shell of polar archaeolipids (PA) extracted from the halophilic archaea *Halorubrum tebenquichense* and Tween 80 [28]. The antioxidant activity of NAC arises from the BR, a lineal C50 polyene with conjugated 13-double bonds, plus two hydroxyl groups at each terminal end, also extracted from *H. tebenquichense* [29]. NAC are also refractory to physical, chemical, and enzymatic attacks because of their *sn* 2,3 ether linked PA shell [28], also responsible for exhibiting ligands for cells expressing SRA1, such as macrophages and certain endothelial cells [30]. By loading dexamethasone within NAC, both its anti-inflammatory activity and the antioxidant activity of BR, were efficiently protected against hostile conditions of simulated gastrointestinal tract [28].

Our hypothesis is that NAC could protect the structure of VD3 and that upon internalization by either activated keratinocytes and activated macrophages, NAC-VD3 could display not only *anti*-hyperproliferative and anti-inflammatory activities but also antioxidant activity. Here, the structural features and *in vitro* activity of NAC-VD3 on $CaCl_2$ differentiated HaCaT cells stimulated with imiquimod (IMQ), to recall the hyperproliferative, inflammatory and oxidative processes implicated in Ps, and on lipopolysaccharide activated macrophages, are presented. Besides, the antibacterial activity of NAC-VD3 is reported for the first time.

2. Materials and methods

2.1. Materials

Compritol ATO 888, soybean phosphatidylcholine (SPC, purity >90%) and Miglyol 840 were gift from Daltosur SRL (Gattefosse), Lipoid (Ludwigshafen, Germany) and Etilfarma SA (Argentina), respectively. Vitamin D3 (VD3) was a gift from Roemmers Argentina. 2,2-diphenyl-1-picrylhydrazyl (DPPH), 6-hydroxy-2,5,7,8-tetramethylchroman-2-carboxylic acid) (Trolox), 3-(4,5-dimethylthiazol-2-yl)-2,5-diphenyl tetrazolium bromide (MTT), crystal violet, 3-(2′-benzothiazolyl)-7-diethylaminocoumarin (coumarin-6, C6) and lipopolysaccharide from *Escherichia coli* O111:B4 (LPS) were from Sigma-Aldrich (MO, USA). 2′,7′-dichlorodihydrofluorescein diacetate (H_2DCFDA) was from Thermo Fisher Scientific, USA. Roswell Park Memorial Institute 1640 (RPMI), Modified Eagle Medium (MEM), Dulbecco's Modified Eagle Medium Nutrient Mixture F-12 (DMEM F-12), penicillin-streptomycin sulphate, glutamine, sodium pyruvate and trypsin/ethylenediamine tetra acetic acid were from Gibco®, Life Technologies (NY, USA). Fetal bovine serum (FBS) was from Internegocios, Cordoba, Argentina. Mueller Hinton broth (MHB), bacteriological agar, bacteriological tryptein and yeast extract was purchased from Britania, Buenos Aires, Argentina. Gentamicin was purchased from Klonal (CABA, Argentina). The other reagents were of analytic grade from Anedra (Buenos Aires, Argentina).

2.2. Archaebacteria growth, polar archaeolipids and BR extraction and characterization

Halorubrum tebenquichense archaeas were grown in 15 l basal medium supplemented with yeast extract and glucose at 40 °C and 600 rpm in a home-made bioreactor and harvested after 96 h growth. Total archaeolipids were extracted using the Bligh and Dyer method modified for extreme halophiles [31], and then separated by cold acetone precipitation into an acetone-insoluble fraction (polar archaeolipids, PA) and acetone soluble fraction (neutral lipids, BR extract). Both fractions were dried and stored at −20 °C until used.

PA was routinely screened by phosphate content [32], and electrospray-ionization mass spectrometry [33]. BR extracts were characterized by UV–visible spectra (300–700 nm) and quantified by absorbance at 490 nm using an average extinction coefficient ($E^{1\%}_{1cm}$) of 2660 [34].

2.3. Preparation and characterization of VD3-nanoparticles (VD3-Nps)

Nanostructured archaeolipid carriers (NAC) made of compritol: BR extract: PA: T80 (2: 2: 1.2: 3% w/w) and nanostructured lipid carriers (NLC) made of compritol: Miglyol: SPC: T80 (2: 2: 1.2: 3% w/w) were prepared as state in Higa et al., 2020 [28] by the emulsion-ultrasonication method. Briefly, 60 mg compritol and 60 mg BR extract or Miglyol were melted at 75–80 °C in a water bath. In another separate tube, 36 mg of TPA or SPC and 90 mg of T80 were suspended in 3 ml of ultra-pure water and heated at 75–80 °C. The aqueous phase was dispersed for 30 s using an Ultra TurraxT10 Basic (IKA, Germany) and immediately added dropwise into the oil phase at 13,000 rpm at 75–80 °C. This hot oil-in-water emulsion was sonicated with a probe-type sonicator (6 mm probe, Sonics & Materials Inc, Vibra Cell Power, USA130 Watt), at 70% amplitude for 10 min. Finally, the

nano-emulsion was cooled down at 4 °C.

To prepare VD3-Nps (NAC-VD3 and NLC-VD3) 10 mg VD3 powder were added to 120 mg of oil phase and processed as stated before. After solidification, Nps were filtered across a nylon syringe filter membrane of 0.45 μm pore size to eliminate free VD3.

To prepare fluorescent labelled Nps, 0.3 mg of the fluorescent hydrophobic dye coumarin-6 (C6) (NAC-C6 and NLC-C6), was mixed with 120 mg of oil phase (0.01% w/w) as described by Higa et al., 2017 [35] and processed as stated for VD3-Nps. After solidification, Nps were filtered across a cellulose acetate filter membrane of 0.45 μm pore size to eliminate free C6.

2.3.1. Size and ζ potential

Size and ζ potential of Nps were determined by dynamic light scattering (DLS) and phase analysis light scattering (PALS) respectively, using a nanoZsizer equipment (Malvern Instruments, Malvern, United Kingdom), after 20-fold dilution in distilled water.

2.3.2. Quantification of VD3, BR and C6

VD3 was quantified by spectrophotometry at 264 nm [36] after complete disruption of Nps in ethanol 96 (1/200). Void Nps was used as blank. The absorbance of the sample was compared to a standard curve prepared with VD3 in ethanol 96. The standard curve was linear in the range 0–50 μg/ml (R^2: 0.9995). Encapsulation efficiency (%EE) was calculated using the following relationship: (amount of VD3 in the filtrate/amount of VD3 added) × 100.

2.3.3. Quantification of BR

BR was quantified measuring the absorbance at 490 nm as state in section 2.2, after complete disruption of Nps in methanol. Void Nps were used as blank.

2.3.4. Quantification of C6

C6 was quantified by fluorescence at λex: 465 nm and λem: 495 nm [37], after complete disruption of Nps in Cl_3CH (1/2000). The fluorescence of the sample was compared to a standard curve prepared with C6 in Cl_3CH. The standard curve was linear in the range 0–25 ng/ml (R^2: 0.99).

2.3.5. Morphology

Morphology of Nps was studied cryo-electron microscopy (cryo-EM). Briefly, samples were prepared in a controlled environment vitrification system (Vitrobot Mark I, FEI, The Netherlands) with controlled temperature (22 °C) and humidity (100%). Samples were examined in Jeol JEM-1400Plus (JEOL, Japan) instrument, operating at 120 kV. Image collections were made using a CCD camera Gatan Multi Scan 794. Sample preparation and data acquisition were performed at the Electron Microscopy Laboratory, Brazilian Nanotechnology National Laboratory.

2.3.6. Thermal analysis

Calorimetric analysis of physical mixture of lipids and aqueous suspension of Nps were performed using a DSC Q200 TA instrument equipped with a Refrigerator Cooling System (RCS90). Briefly, 3–5 mg of lipids or Nps suspension was taken in an aluminium pan. DSC scans were recorded from −50 °C to 90 °C for aqueous suspensions and from −50 °C to 290 °C for bulk material at a heating rate of 10 °C/min, using an empty pan as reference. Melting point and enthalpy were calculated using the software TA Universal analysis provided by TA instruments®. The crystallinity index (C.I.) was calculated according to the following equation: ΔH nanoparticles dispersion (J/g)/[ΔH bulk material (J/g) x concentration lipid phase (%)] x 100 [38].

2.3.7. Raman spectroscopy

Raman spectra were recorded using an i-Raman BWS465 785S, BWTEK equipment, in the Instituto de Investigaciones Fisicoquímicas Teóricas y Aplicadas (INIFTA-CONICET-UNLP). Parameters and conditions were adjusted to obtain the best signal-noise ratio. Samples were measured using aluminium foil baskets to avoid interfering Raman signals from the container. Experimental details: laser $\lambda = 785$ nm, time of each scan: 5.000 mseg, number of scans: 5, *P*out laser: 50–100%

2.3.8. Small angle X-ray scattering (SAXS)

SAXS experiments were carried out using a model XEUSS 1.0 from XENOCS, with beam of RX from Cu Kα 1,2 ($\lambda = 1.54178$ Å) and a sample detector Pilatus100K (DECTRIS, Suiza) in the INIFTA-CONICET-UNLP.

2.3.9. 2,2-Diphenyl-2-picrylhydrazyl (DPPH) radical scavenging assay

DPPH radical scavenging assay was performed as described by Higa et al., 2020 [28]. Briefly, 667 μl of 100 μM $DPPH^{*+}$ in methanol was mixed with 83 μl of sample and incubated for 30 min at 37 °C in the dark on an orbital shaker. Then, the absorbance at 580 nm was measured in a Metrolab 330 spectrophotometer, and the radical scavenging activity (RSA) (%) was calculated as: (Abs negative control -Abs sample)/Abs negative control x 100. Where Abs negative control is the absorbance of 667 μl of DPPH* + 83 μl of methanol. Calibration curves of Trolox (1.2–10 μg/ml) and BR extract were done. The inhibitory concentration of the extract providing 50% reduction of the RSA (IC50) was calculated from a graph built with log RSA (%) against BR concentration.

The antioxidant activity of Nps was measured after extraction in methanol. Briefly, 250 μl of Nps were mixed with 100 μl of methanol. The mixture was then centrifuged at 9500 g for 10 min, the supernatant collected and 100 μl of methanol were added to the pellet. After a second centrifugation, the supernatant was mixed with the first one and dried under flux of N_2.

2.4. VD3 release from Nps

The structural stability of VD3-Nps against dilution at pH 7.4 and pH 5.2 was determined by dialysis. Briefly, one volume of VD3-Nps or VD3 was dialysed along 6 days employing 12.000 MWCO (Sigma-Aldrich, MO, USA) dialysis activated membranes at 35 °C and 80 rpm against 30 vol of release medium (PBS (pH 7,4 or pH 5.2): ethanol 70:30 v/v; to maintain sink conditions [39]. VD3 was quantified every each 24 h in the dialyzed medium as previously described. Size, PDI and ζ potential of samples within the bags were determined.

2.5. VD3 stability in Nps

The stability of VD3-Nps was determined upon incubation at 37 °C in a water bath protected from light for 24 h. VD3 remaining in formulations was quantified by UV-HPLC as described by Temova et al., 2016 with modifications [40]. A Shimadzu Prominence HLPC system equipped with a PDA detector and a reverse phase column (Synergi Polar-RP (ether-linked phenyl phase with polar end capping, 150 Å, 75 mm × 4.6 mm, 4 μm, Phenomenex) was used. A mixture of A: formic acid 1 %v/v and B: methanol (isocratic 10% A, 90% B) was applied as the mobile phase at a flow rate of 0.6 ml/min. The injection volume was 25 μl and the detection wavelength was set at 260 nm. Standard calibration curves were prepared from 0.2 to 1 mg VD3/ml in ethanol (R^2: 0.99970).

2.6. Stability of VD3-Np upon storage

The colloidal stability of VD3-Nps was determined after 6-months of storage at 4 °C. Nps size, PDI and Z potential before and after storage were determined as stated before.

2.7. Cell lines and culture conditions

Human keratinocytes (HaCaT cells) were cultured in MEM supplemented with 10% FBS, 1% antibiotic-antimycotic and 2 mM L-glutamine. Human monocyte cell line THP-1 (ATCC TIB- 202™) was maintained in RMPI medium supplemented with 100 U/ml penicillin,

100 μg/ml streptomycin and 2 mM L-glutamine, 0.05 mM 2-mercaptoethanol and 1 mM sodium pyruvate. THP-1, monocytes, were differentiated into macrophages by treatment with 100 ng/ml PMA for 24 h. Both cell lines were grown in a humidified atmosphere of 5% CO_2 at 37 °C.

2.7.1. Cell viability

Cell viability upon 24 h incubation with void or VD3-Nps was measured by MTT assay according to Mosmann et al., 1983 with modifications [41]. Briefly, THP-1 and HaCaT cells were seeded in 96-well plates at a density of 4×10^4 cells per well and grown for 24 h. Then, cells were incubated with series of different concentration of void Nps (20, 200 and 2000 μg compritol/ml), and VD3-Nps (3.7–5, 37–50 and 370–500 μg VD3/ml - 20, 200 and 2000 μg compritol/ml, respectively). After 24 h of incubation the medium was removed, cells were washed with PBS and 110 μl of 5 mg/ml MTT solution was added to each well. After 3 h of incubation, the MTT solution was removed, the insoluble formazan crystals were dissolved with 100 μl of dimethyl sulfoxide, and absorbance was measured at 570 nm in a microplate reader (Dynex Technologies, MRX tc, Chantilly, Virginia). The cell viability was expressed as a percentage of the cells grown in medium.

2.7.2. Induction of a psoriatic phenotype on HaCaT cells (Ps cell model)

A psoriatic cell model made of $CaCl_2$ differentiated-imiquimod (IMQ) stimulated HaCaT cells was stablished as state by Li et al., 2013 [2]. Briefly, HaCaT cells were seeded at a density of 3×10^4 cells/well in 96-well plates in DMEM F12 medium supplemented with 2.5% inactivated FBS, 1% L-glutamine and 1% antibiotic-antimycotic. After 24 h incubation, fresh medium containing 2 mM $CaCl_2$ were added and further incubated for 48 h. Then, 100 μM IMQ was used to induce psoriatic like inflammation in differentiated HaCaT cells for 48 h or 120 h. Non-stimulated HaCaT cells were used as control.

2.7.3. Cell proliferation assay

Non-stimulated HaCaT cells and Ps cell model was treated with VD3, void Nps and VD3-Nps at 20 μg compritol/ml-3.7–5 μg VD3/ml for 48 or 5 days and the cell viability was determined by MTT assay, as state in section 2.7.1.

2.7.4. Anti-inflammatory and antioxidant activity

Anti-inflammatory and antioxidant activity of VD3-Nps on the Ps cell model were determined by measuring the production of IL-8 and ROS. Briefly, upon VD3 and VD3-Nps incubation, supernatants of cells were collected and stored at −20 °C for further analysis. IL-8 was measured by enzyme-linked immunosorbent assay (ELISA) (BD, OptEIA, BD Biosciences, CA, USA), following the manufacturer instructions. On the other hand, the generation of ROS was measured on the attached cells using the carboxy-H2DCFDA dye. Briefly, cells attached at the bottom of the well were incubated with 13 μM carboxy-H2DCFDA for 30 min at 37 °C. After incubation, the cells were trypsinized, washed with PBS and 1×10^5 cells were analysed by flow cytometry (λEx/Em: 492–495/517–527 nm) (BD FACSCalibur™; BD Biosciences, San Jose, CA, USA). Data were analysed using WinMDI 2.9 software (Microsoft, Redmond, WA, USA).

2.7.5. Cellular uptake

The uptake of C6-labelled Np was measured by flow cytometry on non-stimulated HaCaT cells and on the Ps cell model. Briefly, non-stimulated HaCaT cells and Ps cell model, seeded in 24-well plates at a density of 2×10^5 cells per well, were then incubated with 20 μg compritol/ml Nps-C6 for 1 and 4 h. After incubation, the cells were trypsinized, washed with PBS and 1×10^4 cells were analysed by flow cytometry. The fluorescence was normalized to the C6 content of each formulation.

2.8. IL-8 release, ROS induction and CD204 expression on LPS stimulated THP-1 cells

Differentiated THP-1 cells were seeded at 6×10^4 cells/well in 48-well plates and grown for 24 h at 37 °C.Then, cells were incubated with fresh medium with 5% FBS containing VD3 (5 μg/ml) void Nps (20 μg compritol/ml) or VD3-Nps (20 μg compritol/ml 3.7–5 μg VD3/ml) with and without 1 μg/ml of LPS. After 24 h of incubation, supernatants were collected and stored at −20 °C until analysis, and cells on each well were trypsinized, washed with PBS and resuspended in 100 μl PBS added with 3 μl of anti-CD204 antibody (CD204 Monoclonal Antibody (PSL204), APC, eBioscience, Invitrogen Thermo Fisher Scientific), followed by 30 min incubation in the dark. After centrifuging at 2240 g for 5 min, the supernatant was discarded, cells resuspended in 300 μl of PBS and analysed by flow cytometry as stated before. Human IL-8 was measured by ELISA in supernatants and the generation of ROS was measured on the attached cells using the carboxy-H2DCFDA dye as state before.

2.9. Antibacterial activity

2.9.1. Bacterial strains and growth conditions

The reference *Staphylococcus aureus* American Type Culture Collection (ATCC) 25923 was grown in Lysogeny Broth (LB) at 37 °C with shaking at 200 rpm overnight before testing.

2.9.2. Antibacterial activity on planktonic S. aureus

The growth of *S. aureus* after 24 h of incubation with gentamicin, VD3, VD3-Nps, void Nps and BR extract was determined by optical density (OD) at 595 nm and by counting the colony forming units (CFU). Briefly, two-fold dilutions of samples were prepared in MHB, and 80 μl were added to wells in 96-well plate. Subsequently, 20 μl of bacterial inoculum at 1×10^8 CFU/ml was added to each well. Immediately and 24 h after incubation at 37 °C, OD was measured. Then, 50 μl of first and second dilution were inoculated onto nutrient agar plates in triplicate. The plates were incubated overnight at 37 °C, colonies were counted, and the results obtained expressed as $\log_{10}$ CFU/ml. Inoculum in MHB was used as control without treatment and gentamicin was used as standard positive control. Each sample was assayed in triplicate and in two independent experiments. The minimum inhibitory concentration (MIC) was defined as the lowest concentration of samples that inhibits 90% growth respect to the control in MHB.

2.9.3. Effect on biofilm formation

Inhibition of biofilm formation was determined according to Mishra & Wang, 2017 [42]. Supernatants of the microplate of growth experiment were removed and the biomass of biofilm was determined by staining with crystal violet. Briefly, after two washes with sterile PBS, the plate was dried at 37 °C, and biofilm was fixed with methanol for 15 min. Then, methanol was removed, the plate was dry, and 0.1% w/v crystal violet was added. After 20 min, two washes were carried out with distilled water and the plate was again dry. Subsequently, stains were solubilized with 30% v/v acetic acid and absorbance of crystal violet at 595 nm (AbsCV) was measured. The percentage of biofilm inhibition was calculated as follows: $100 - (AbsCV_{sample}/AbsCV_{control} * 100)$ where $AbsCV_{sample}$ is AbsCV after *S. aureus* incubation with sample and $AbsCV_{control}$ is AbsCV of control without treatment.

2.10. Statistical analysis

Statistical analyses were performed by one-way analysis of variance followed by Dunnet's test or two-way analysis of variance followed by Sildak's test using Prisma 4.0 Software (Graph Pad Software, CA, USA). The p-value of <0.05 was considered statistically significant: $*p < 0.05$; $**p < 0.01$; $***p < 0.001$, $****p < 0.0001$; n.s. represents non-significant ($p > 0.05$).

3. Results

3.1. Structural features of VD3-Nps

The structural features of void and VD3-Nps are shown in Table 1. VD3 incorporation did not change of size of NAC but significantly increased the size of NLC, resulting the size of NAC-VD3 nearly six times smaller than that of NLC-VD3 (~70 nm vs ~ 400 nm). The presence of polar archaeolipids in NAC-VD3, resulted in highly negative ζ potential compared to that of NLC-VD3 (−39 mV vs −16 mV). The encapsulation efficiency was 49 ± 11% and 37 ± 14% for NAC-VD3 and NLC-VD3, respectively, suggesting that BR within NAC core, favoured VD3 encapsulation. VD3 solubility was increased by ~13 folds and by ~9 folds within NAC-VD3 and NLC-VD3 respectively. NAC and NAC-VD3 suspensions showed the typical red colour of BR (Fig. S1). Cryo-EM images of NAC-VD3 showed different morphologies such as < 100 nm circular and 50–100 nm needle like shapes of higher electron density. NLC-VD3 was observed as > 200 nm circular structures (Fig. S2).

In NAC, possessing a core made of solid compritol: semisolid BR extract (50:50 w:w), the compritol crystallinity was decreased by 10% (Table S1). The thermograms showed a small peak below 0 °C that could be attributed to BR extract forming lacunae within solid compritol (Fig. S3A). In NAC-VD3 instead, the compritol crystallinity was strongly decreased to a 30% while the peak below 0 °C disappeared. This suggests that VD3 may be trapped the compritol-BR core, the BR extract playing a role in such interaction, resulting in an important structural distortion of the core [43]. NAC-VD3 also showed a reduced enthalpy compared to NAC. Such reduction may be owed to the presence of VD3 in the core, where BR would facilitate its trapping.

In NLC on the other hand, the compritol crystallinity was reduced by 20%, and the thermograms showed 2 peaks below 0 °C, attributed to Miglyol (Fig. S3B). In NLC-VD3, the compritol crystallinity was reduced to 45%, and the peaks below 0 °C were maintained. This suggests that VD3 would be dissolved, either total or partly within the Miglyol lacunae; the solid matrix thus would experience less distortion than in NAC-VD3. Finally, NLC-VD3 experienced also reduced enthalpy compared to NLC tough of lower magnitude than NAC-VD3.

Taken together, these results suggest that the trapping of small hydrophobic molecules within the core may be favoured by the presence of BR extract.

The structure of NAC-VD3 was also assessed by SAXS. The crystalline compritol is known to exhibit a periodicity of Bragg reflections with ratios close to 1, 2, 3, and 4, and lattice spacings calculated at 6.26–6.86 nm [44,45]. SAXS spectra of NAC-VD3 showed a single scattering peak (Fig. S4), indicating a lower compritol lamellarity in the core, compared to bulk compritol; and a reduction the lattice spacing compared to NAC (from 6.5 nm to 6.4 nm). Similar trend was found in the SAXS spectra of NLC-VD3, with higher decrease of lattice spacing from 6.4 nm to 6.1 nm for NLC and NLC-VD3, respectively. Suggesting that VD3 promoted the approximation between compritol lamellae.

Table 1
Structural features of nanoparticles.

Sample	Mean diameter (nm ± SD)	PDI	ζ potential (mV ± SD)	VD3 (mg/ml ± SD)	BR (μg/ml ± SD)
NLC	192.8 ± 68.4	0.225 ± 0.05	−14.7 ± 5.5	–	–
NAC	80.9 ± 19.5	0.35 ± 0.12	−42.3 ± 12.7	–	0.34 ± 0.2
NLC-VD3	420 ± 200	0.45 ± 0.25	−16.1 ± 5.2	3.7 ± 1.4	–
NAC-VD3	70.1 ± 11.4	0.315 ± 0.11	−38.9 ± 7.1	4.9 ± 1.1	0.35 ± 0.15

Data are expressed as mean ± standard deviation (SD) from twelve independent batches.

The Raman spectral peaks of compritol, BR and VD3 agreed with previous reports (Fig. 1; Table S2) [46,47]. The signals from compritol in NAC and NAC-VD3 were comparable to those from crystalline compritol, excepting the less pronounced splitting of the CH_2 scissoring band (1438 cm^{-1}), indicating an interaction between the hydrocarbon chains from compritol in NAC with BR (or with BR and VD3 in NAC-VD3). On the other hand, the signals from BR in NAC, suffered important modifications compared to bulk BR: the C═CH deformation peak (1000 cm^{-1}) was reduced and broadened, the C–C stretching peak (1151 cm^{-1}) was shifted to higher wavenumbers (1154 and 1156 cm^{-1} respectively), and the C═C stretching peak (1509 cm^{-1}) was reduced and broadened. These results suggest a reduction in the movement freedom of the methylene groups from BR, whose polyenic chains would be immobilised by the compritol. Finally, NAC-VD3 showed the same BR peak pattern of NAC, of lower intensity, besides of a reduction in the intense peak of C═C stretching (1650 cm^{-1}) of VD3, suggesting a potential association/immobilization of VD3 within the compritol-BR core.

Raman signals from compritol in NLC and NLC-VD3 were very weak due to the presence of the liquid lipid Miglyol [48]. In NLC-VD3, the stretching modes of CH_2 were shifted to higher wavenumber; a less pronounced splitting of the CH_2 scissoring band was observed compared with NLC, and the remaining bands of compritol were broadened. A small shoulder at 1650 cm^{-1} ascribed to VD3, was also observed.

3.2. Antioxidant activity

The antioxidant activity showed the following trend: NAC-VD3> NAC > BR. VD3 alone and NLC-VD3, on the other hand, had no antioxidant activity (Table S3). The antioxidant activity of BR extract was increased when loaded in NAC, and remarkably, the inclusion of VD3 in the core, duplicated it.

3.3. Degradation of VD3

Upon 24 h incubation at 37 °C, the 100% of VD3 was conserved within NAC-VD3. Instead, either dissolved in ethanol or loaded within NLC-VD3, it experienced almost complete degradation (Fig. S5).

3.4. VD3 release from Nps

Upon submitted to a 3-fold dilution for 6 days at pH 7.4, a 15% loss of VD3 content and a ~7-fold increase on size and PDI was experienced by NAC-VD3, while maintaining its nanometric size. On the other hand, a 35% loss of VD3 content, together with a significant increase of ~15 folds on size and PDI was experienced by NLC-VD3 (Fig. 2 A and B). Similar trend was found upon submitted to a 3-fold dilution for 6 days at

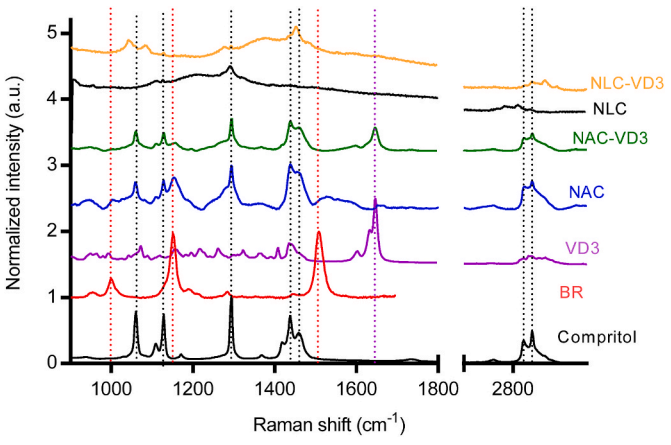

Fig. 1. Raman spectra of compritol, BR, VD3, NAC, NAC-VD3. NLC and NLC-VD3.

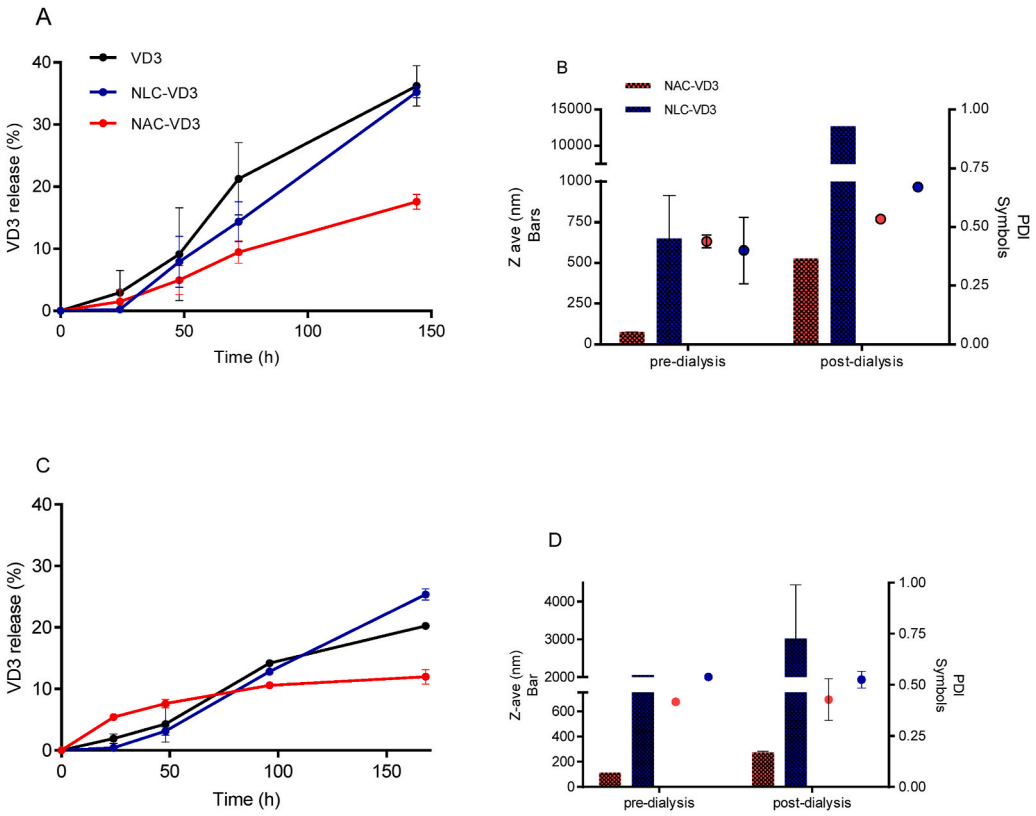

Fig. 2. VD3 release upon nanoparticles incubation at pH 7.4 (A and B) and pH 5.2 (C and D) at 37 °C. (A) VD3 release from NLC-VD3 and NAC-VD3 after 6 days of dialysis (A and C) and (B and D) size and polydispersity (PDI) of nanoparticles before and after dialysis. Values are expressed as mean ± SD (n = 3).

pH 5.2 (pH of psoriatic skin [49]), except that 11%, 25% and 20% of VD3 was lost upon 6 days incubation by NAC-VD3, NLC-VD3 and VD3, respectively (Fig. 2 C). A ~2-fold increase on size and PDI was experienced by NAC-VD3 while ~3 -fold increase on size was experienced by NLC-VD3.

3.5. Structural stability of Np upon storage

Upon 6 months storage at 4 °C, the mean size and PDI of NAC-VD3 was retained, while the colloidal stability of NLC-VD3, as judged by its increased mean size and PDI, was lost (Fig. S6).

3.6. Cell viability of keratinocytes and THP-1 derived macrophages

Keratinocytes endured with >75% viability, up to 0.2 mg compritol/ml from NAC that for NAC-VD3 represented 40 μg VD3/ml (Fig. S7). Remarkably 40 μg/ml of VD3 alone, resulted extremely toxic. The cytotoxicity of NLC/NLC-VD3 on keratinocytes instead, was slightly higher. On the other hand, the cytotoxicity of NAC/NAC-VD3 on THP-1 macrophages also presented a limit at 0.2 mg compritol/ml and followed a profile like that of keratinocytes, excepting that 40 μg VD3/ml were not harmful, indicating a higher sensitivity of keratinocytes to VD3.

3.7. Cellular uptake, antiproliferative activity, IL-8 release and ROS induction in the psoriatic cell model

The extent of uptake was higher for NAC-C6 than for NLC-C6 at 1 and 4 h by both non-differentiated HaCat cells and by the Ps cell model (Fig. 3), being 3.5-fold higher upon 4 h incubation on the Ps cell model. As expected, at nontoxic concentration (0.02 mg compritol/ml and 3.7–5 μg VD3/ml) after 48 h neither Nps not VD3 decreased the viability/proliferation of non-differentiated HaCat cells. Instead, the cell proliferation in the Ps model was reduced 50% by NAC-VD3 and 30% by NLC-VD3, that increased to 65 and 40% respectively, upon 5 days of incubation (Fig. 4). However, upon 5 days of incubation, viability of non-differentiated HaCat cells was also reduced, and VD3 reduced

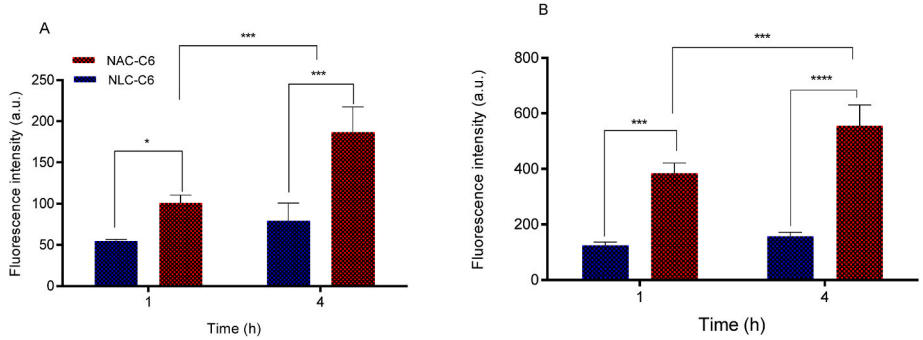

Fig. 3. Uptake of NLC-C6 and NAC-C6 in HaCaT cells (A) and Ps cell model (B). Values are expressed as mean ± SD (n = 3).

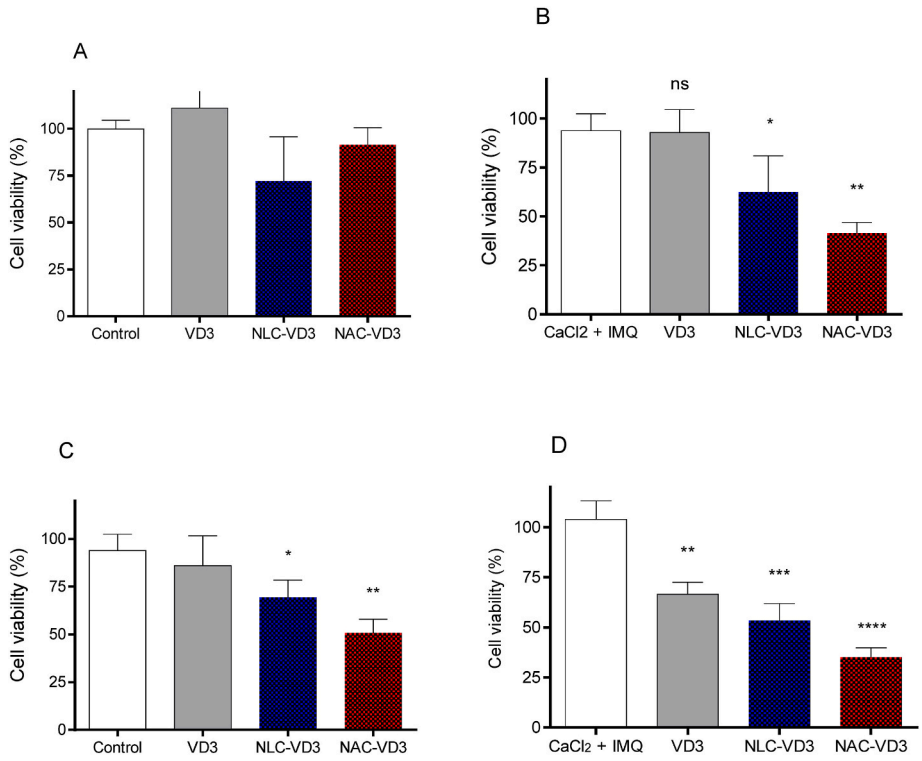

Fig. 4. Viability of non-differentiated cells (A and C) and Ps cell model (B and D) after 48 h (A and B) and 5 days of incubation (C and D).

~30% viability of Ps cell model. Importantly, NAC-VD3 significantly reduced the release of IL-8 and ROS generation on the Ps model to levels of non-differentiated HaCaT cells (Fig. 5).

3.8. IL-8 release, ROS induction and CD204 expression on LPS stimulated THP-1 macrophages

NAC-VD3 reduced IL-8 release and ROS production on THP-1 LPS stimulated (Fig. 6). Besides, NAC-VD3 blocked the enhanced expression of CD204 induced by LPS but does not affect the basal expression of CD204 (Fig. S8).

3.9. Activity against S. aureus

Gentamicin showed high anti *S. aureus* activity (MIC: 2 μg/ml, and complete inhibition of biofilm formation at 1 μg/ml). Neither NLC, NAC, VD3-Nps, nor VD3 showed any antibacterial activity. Besides, their combination with gentamicin did not modify the antibiotic activity. Interestingly, BR extract showed antibacterial activity. We found a reduction of bacterial growth (3–7 $\log_{10}$) after 24 h of incubation with 70 μg/ml of BR and an inhibition of 90 ± 1.6% of biofilm formation (Fig. S9).

4. Discussion

VD3 is a small (384.64 Da molecular weight) lipophilic (log P value of 7.5), poorly water-soluble molecule (0.38 μg/ml), with *in vitro* anti-psoriatic activity, but that upon topical delivery rapidly oxidises before reaching target cells. VD3 has been formulated in Nps to avoid its oxidation [50]. However, the preparation methods used require high temperatures or toxic solvents, which can damage the VD3 structure [51]. Significant stabilization of VD3 has been achieved by including traditional antioxidants such as butylhydroxytoluol (BHT), EDTA, citric acid, and ascorbic acid within Nps [52]. However, up to now VD3 has not been loaded within NAC. Here, we hypothesized that NAC would protect the VD3 structure, while increasing antiproliferative, anti-inflammatory and antioxidant activity. Besides not requiring organic solvents for their preparation, NAC display unique structural features that make them attractive compared to other types of lipid Nps. Their surface contains Tween 80 and PA, a mixture of *sn* 2,3 ether linked

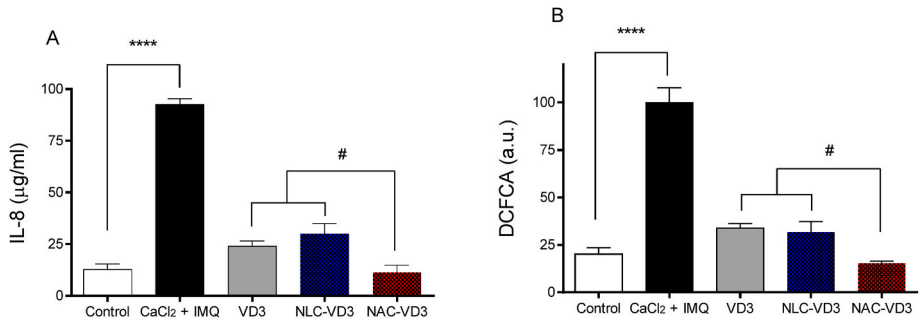

Fig. 5. Anti-inflammatory and antioxidant activity on the Ps cell model upon 5 days incubation with VD3 and VD3-Nps. (A) IL-8 release and (B) Fluorescence intensity of carboxy-DCFDA. Values are expressed by mean value ± S.D (n = 3). * Significant differences with control cells. # Significant differences between treatments.

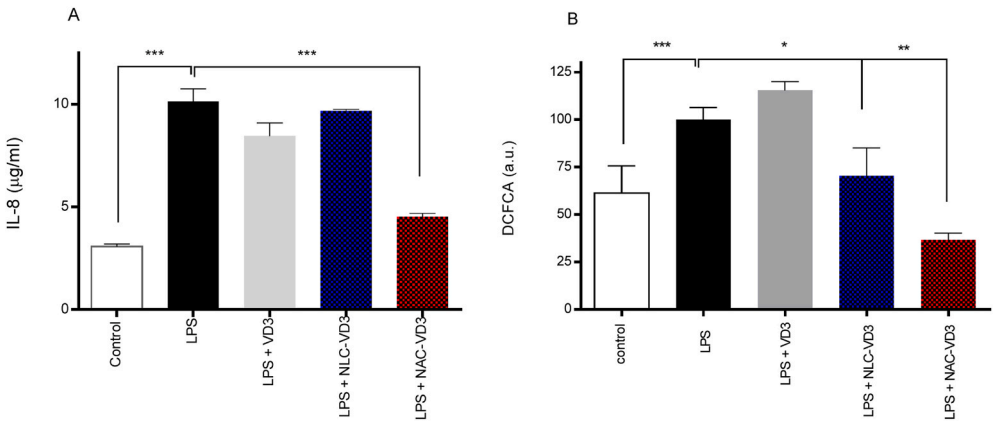

Fig. 6. IL-8 (A) and ROS (B) production by LPS stimulated THP-1 cells.

phytanyl saturated archaeolipids extracted from the halophilic archaebacteria *H. tebenquichense*. Because of its PA in surface, NAC (and drugs loaded therein) become refractory to hydrolysis, oxidation, and stereospecific phospholipases [53], being PA responsible for the small size, high negative ζ potential and colloidal stability of NAC [28]. In addition, the NAC core is made of compritol and BR extract. BR is a RNS and ROS scavenger and quencher of singlet oxygen [54,55], acknowledged as a potent natural antioxidants [28]. Various studies have shown BR potential applications as antioxidant, antihaemolytic [56], antimicrobial [57–59]) anticancer and antiviral [60]. Moreover, beneficial effects on sperm cells viability [61] and cholinesterase inhibition activity has been reported [62]. BR could prevent skin cancer, since it can repair damage in DNA strands that occurs after exposure to ultraviolet radiation [63]. Bacterioruberin is commercialized by Halotek in Germany as a skin-protective ingredient in personal care products and as an effective antioxidant, providing a natural alternative to synthetic antioxidants such as BHT [64].

Here first, we introduced the structural features of NAC-VD3. DSC thermograms and SAXS spectra of NAC-VD3, showed that VD3 was trapped within a disordered core, being its aqueous solubility slightly (~1.3 folds) higher than in NLC-VD3 (comparable to polymeric Nps [50]) but 13 folds higher than VD3 water solubility. Besides, VD3 was more efficiently retained within NAC-VD3 than in NLC-VD3 when diluted at pH 7.4 and 5.2, and remarkably, it was protected against thermal degradation. The small size of NAC-VD3 would enhance their occlusive potential *in vivo* [65], which reduces *trans*-epidermal water loss, improves hydration, and increases drug penetration. On the other hand, VD3 improved the antioxidant activity of BR in NAC-VD3, surpassing that of BR alone or in NAC, suggesting the existence of synergy between BR and VD3.

In second place, we tested the effect of NAC-VD3 on a psoriatic cell model based on keratinocytes, that after Ca^{+2} mediated differentiation, expresses TLR7 in response to IMQ. IMQ, an analogue of adenosine, induces psoriasiform dermatitis in humans and mice when applied topically, and pro-inflammatory cytokines on keratinocytes [2,66,67]. IMQ is a ligand for TLR7 and TLR8; it induces nuclear translocation of NF-kB in keratinocytes, and further production of IL-8, IL-6, TNF-α, IL1β, macrophage inflammatory protein-3a, also known as C–C Motif Chemokine Ligand 20 (CCL20) and cutaneous T-cell-attracting chemokine (CTACK/CCL27) [2]. After 48 h of incubation on the Ps cell model, NAC-VD3 displayed higher anti-proliferative activity than NLC-VD3 and VD3 alone. The higher antiproliferative activity of NAC-VD3 may have ascribed to its extensive intracellular uptake, which after 4 h was 3.5 times higher than that of NLC-VD3. On the contrary, neither VD3-Nps (despite its extensive internalization) not VD3 affected non-differentiated keratinocytes. In the Ps cell model, remarkably, NAC-VD3 showed the highest antioxidant activity. Besides, the anti-inflammatory and antioxidant activity of VD3, in terms of inhibiting IL-8 and ROS production, were magnified by NAC-VD3.

In third place, the effect of NAC-VD3 on LPS activated human macrophages was tested. Recruitment and activation of macrophages in psoriatic skin lesions and blood vessels is a key step towards uncontrolled inflammation [68,69]. Oxidative stress contributes to immunological abnormality and development of psoriasis [70]. ROS induce the release of inflammatory factors that stimulate keratinocyte proliferation and angiogenesis, and directly damage the vascular endothelium, inducing vascular inflammation. Macrophages release TNF-α, IL-6, IL-1β, and IL-8 that facilitate the recruitment of inflammatory cells [71] We have previously determined that macrophages internalize NAC in higher extent than NLC [28]. Such internalization is mediated by PGP-Me (the most abundant PA extracted from *H. tebenquichense* [33], which is a ligand for SRA1 expressed by macrophages and endothelial cells [30]. Here, we observed that LPS increased the SRA1 expression on THP-1 macrophages, suggesting that a massive NAC-VD3 internalization is expected by activated macrophages. SRA1 is also responsible for inhibiting the response to LPS triggered by TLR4, by inhibiting the NFkb pathway [72,73]. The anti-inflammatory activity of SRA1 ligands was evidenced here, by the efficient reduction of IL-8 secretion caused by NAC-VD3 on LPS activated macrophages. On the other hand, NAC-VD3 also reduced ROS production. Despite of the expression of SRA1 on activated keratinocytes has not been reported, the anti-inflammatory activity of NAC-VD3 observed here, would also be mediated by SRA1. Overall, the results are important since the inhibition of IL-8, is considered of significant therapeutic interest [74].

Finally, we tested the antibacterial activity of NAC-VD3. Compared to healthy individuals Ps patients suffer an increased risk for staphylococcal spp colonization. Although, different to atopic dermatitis, the skin of psoriatic patients does not show a defined microbiome, *Streptococcus*, *Corynebacteria* and *Burkholderia* colonize the psoriatic skin and may worsen the disease [75,76]. In addition, *S. aureus* is considered a pathogenic factor of Ps, since it increases Th17 polarization and exacerbates cutaneous inflammation during early colonization of new-born mouse skin [77].

Recent studies showed that VD3 exerts direct bactericidal activity against *Streptococcus mutants* [78]. Besides, its combination with amikacin, neomycin, and gentamicin lowers their MIC by more than 4- folds on clinical multi-drug resistant *Pseudomona aeruginosa*, *E. coli*, and *S. aureus* strains [78]. On the other hand, we have recently reported that archaeosomes containing Thymus vulgaris essential oil display higher antibacterial activity (lower MIC_{90} against planktonic bacteria and higher antibiofilm formation capacity) than Thymus vulgaris essential oil Tween 80 emulsion or liposomes against *S. aureus* ATCC 25923 and four clinical methicillin-resistant *S. aureus* isolates (MRSA) [79]. Here, VD3 or NAC-VD3, alone or combined with gentamicin, were ineffective against MRSA; however, a prominent *anti-S. aureus* activity and *anti*--biofilm formation were displayed by the BR extract at 70 µg/ml.

Carotenoids extracts from *Halorubrum* sp. [80], *Haloarcula hispanica* HM1 and *Halobacterium salinarum* HM2 [81] were recently reported to display moderate inhibitory effect on pathogenic bacteria such as *E. coli*, *Klebsiella pneumoniae*, *P. aeruginosa* and *S. aureus*. Not surprisingly, NAC-VD3 did not show any antibacterial activity. This should be owed to the low bioavailability of BR, which is trapped within the lipid core. Such bioavailability, however, is expected to be increased upon the BR release once the NAC-VD3 transition to gel phase occurring after topical application [82].

5. Conclusions

In this work we showed that VD3 loaded in ultra-small sized, low PDI and highly negative ζ potential NAC, presented good colloidal stability for at least 6 months at 4 °C; the presence of BR within the core aided to trap VD3, protecting it from thermal degradation and avoiding its fast release. NAC-VD3 combined structural protection supplied by PA in surface, with enhanced antioxidant activity of VD3 provided by BR; as a result, its anti-inflammatory and antiproliferative effect on a psoriatic cell model, and on inflammatory macrophages was improved. We observed also that BR was impaired to exert its expected *anti-S. aureus* planktonic and *anti*-biofilm activity, which was negligible for NAC-VD3, but not for free BR. This was probably owed to the strong structural protection provided by NAC structure to BR itself, that avoided a direct contact of BR with bacteria. Such protection, however, would gradually vanish after a given time on the skin surface. Taken together, these preliminary results suggest that NAC-VD3 deserve further deeper exploration, particularly on an *in vivo* Ps model.

CRediT authorship contribution statement

Yamila Roxana Simioni: Methodology, Formal analysis, Writing – original draft. **Noelia Soledad Perez:** Methodology. **Leandro R.S. Barbosa:** Methodology. **Ana Paula Perez:** Methodology. **Priscila Schilrreff:** Methodology, review, Writing – review & editing. **Eder Lilia Romero:** Formal analysis, Writing – original draft, Funding acquisition. **Maria Jose Morilla:** Conceptualization, Supervision, Writing – review & editing, Funding acquisition.

Declaration of competing interest

The authors declare that they have no known competing financial interests or personal relationships that could have appeared to influence the work reported in this paper.

Acknowledgements

This work was financially supported by ANPCYT under Grant PICT 2016-4562 and Secretaria de Investigaciones, Universidad Nacional de Quilmes, under Grant Programa de Nanomedicinas-2. YS and NSP have a fellowship from National Council for Scientific and Technological Research (CONICET). APP, PS, ELR and MJM, are members of the Research Career Program from CONICET. Research supported by LNNano – Brazilian Nanotechnology National Laboratory, CNPEM/MCTI) during the use of the Cryo-TEM open access facility.

Appendix A. Supplementary data

Supplementary data to this article can be found online at https://doi.org/10.1016/j.jddst.2022.103455.

References

[1] C. Albanesi, S. Madonna, P. Gisondi, G. Girolomoni, The interplay between keratinocytes and immune cells in the pathogenesis of Psoriasis, Front. Immunol. 9 (2018) 1549, https://doi.org/10.3389/fimmu.2018.01549.

[2] Z.J. Li, et al., Roles of TLR7 in Activation of NF-κB signaling of keratinocytes by imiquimod, PLoS One 8 (10) (2013), https://doi.org/10.1371/journal.pone.0077159.

[3] M.A. Lowes, M. Suárez-Fariñas, J.G. Krueger, Immunology of psoriasis, Annu. Rev. Immunol. 32 (2014), https://doi.org/10.1146/annurev-immunol-032713-120225.

[4] C.E.M. Griffiths, A.W. Armstrong, J.E. Gudjonsson, J.N.W.N. Barker, Psoriasis, Lancet 3 (397) (2021) 1301–1315, https://doi.org/10.1016/S0140-6736(20)32549-6.

[5] S. Hsu, et al., Consensus guidelines for the management of plaque psoriasis, Arch. Dermatol. 148 (1) (2012), https://doi.org/10.1001/archdermatol.2011.1410.

[6] S.P. Cannavò, G. Riso, M. Casciaro, E. Di Salvo, S. Gangemi, Oxidative stress involvement in psoriasis: a systematic review, Free Radic. Res. 53 (8) (2019), https://doi.org/10.1080/10715762.2019.1648800.

[7] J. Pleńkowska, M. Gabig-Cimińska, P. Mozolewski, Oxidative stress as an important contributor to the pathogenesis of psoriasis, Int. J. Mol. Sci. 21 (17) (2020), https://doi.org/10.3390/ijms21176206.

[8] M. Milani, A. Sparavigna, Antiaging efficacy of melatonin-based day and night creams: a randomized, split-face, assessor-blinded proof-of-concept trial, Clin. Cosmet. Invest. Dermatol. 11 (2018), https://doi.org/10.2147/CCID.S153905.

[9] F. Benhadou, Di Mintoff, V. Del Marmol, Psoriasis: keratinocytes or immune cells - which is the trigger? Dermatology 235 (2) (2019) https://doi.org/10.1159/000495291.

[10] J.K. Salmon, C.A. Armstrong, J.C. Ansel, The skin as an immune organ, West. J. Med. 160 (2) (1994), https://doi.org/10.1002/9781119680642.ch1.

[11] K. Sugita, K. Kabashima, K. Atarashi, T. Shimauchi, M. Kobayashi, Y. Tokura, Innate immunity mediated by epidermal keratinocytes promotes acquired immunity involving Langerhans cells and T cells in the skin, Clin. Exp. Immunol. 147 (1) (2007), https://doi.org/10.1111/j.1365-2249.2006.03258.x.

[12] B.J. Nickoloff, L.A. Turka, Immunological functions of non-professional antigen-presenting cells: new insights from studies of T-cell interactions with keratinocytes, Immunol. Today 15 (10) (1994), https://doi.org/10.1016/0167-5699(94)90190-2.

[13] V.K. Rapalli, G. Singhvi, S.K. Dubey, G. Gupta, D.K. Chellappan, K. Dua, Emerging landscape in psoriasis management: from topical application to targeting biomolecules, Biomed. Pharmacother. 106 (2018), https://doi.org/10.1016/j.biopha.2018.06.136.

[14] K. Rønholt, L. Iversen, Old and new biological therapies for psoriasis, Int. J. Mol. Sci. 18 (11) (2017), https://doi.org/10.3390/ijms18112297.

[15] D.M.W. Balak, Fumaric acid esters in the management of psoriasis, Psoriasis Targets Ther. 5 (2014), https://doi.org/10.2147/PTT.S51490.

[16] M. Czarnecka-Operacz, A. Sadowska-Przytocka, The possibilities and principles of methotrexate treatment of psoriasis - the updated knowledge, Postępy Dermatologii i Alergologii 31 (6) (2014), https://doi.org/10.5114/pdia.2014.47121.

[17] C. Kromer, D. Celis, D. Sonntag, W.K. Peitsch, Biologicals and small molecules in psoriasis: a systematic review of economic evaluations, PLoS One 13 (1) (2018), https://doi.org/10.1371/journal.pone.0189765.

[18] E.J. Samarasekera, L. Sawyer, D. Wonderling, R. Tucker, C.H. Smith, Topical therapies for the treatment of plaque psoriasis: systematic review and network meta-analyses, Br. J. Dermatol. 168 (5) (2013), https://doi.org/10.1111/bjd.12276.

[19] M. Umar, K.S. Sastry, F. Al Ali, M. Al-Khulaifi, E. Wang, A.I. Chouchane, Vitamin D and the pathophysiology of inflammatory skin diseases, Skin Pharmacol. Physiol. 31 (2) (2018), https://doi.org/10.1159/000485132.

[20] L. Barrea, et al., Vitamin D and its role in psoriasis: an overview of the dermatologist and nutritionist, Rev. Endocr. Metab. Disord. 18 (2) (2017), https://doi.org/10.1007/s11154-017-9411-6.

[21] L.K.A.M. Leal, et al., Vitamin D (VD3) antioxidative and anti-inflammatory activities: peripheral and central effects, Eur. J. Pharmacol. 879 (2020), 173099, https://doi.org/10.1016/j.ejphar.2020.173099.

[22] J.M. Ballard, L. Zhu, E.D. Nelson, R.A. Seburg, Degradation of vitamin D3 in a stressed formulation: the identification of esters of vitamin D3 formed by a transesterification with triglycerides, J. Pharm. Biomed. Anal. 43 (1) (2007), https://doi.org/10.1016/j.jpba.2006.06.036.

[23] Y.H. Su, J.Y. Fang, Drug delivery and formulations for the topical treatment of psoriasis, Expet Opin. Drug Deliv. 5 (2) (2008), https://doi.org/10.1517/17425247.5.2.235.

[24] U.U. Mohd Nordin, N. Ahmad, N. Salim, N.S. Mohd Yusof, Lipid-based nanoparticles for psoriasis treatment: a review on conventional treatments, recent works, and future prospects, RSC Adv. 11 (46) (2021), https://doi.org/10.1039/d1ra06087b.

[25] J. Pardeike, A. Hommoss, R.H. Muller, Lipid nanoparticles (SLN, NLC) in cosmetic and pharmaceutical dermal products, Int. J. Pharm. 366 (2009), https://doi.org/10.1016/j.ijpharm.2008.10.003.

[26] E.B. Souto, R.H. Muller, Cosmetic features and applications of lipid nanoparticles (SLN, NLC), Int. J. Cosmet. Sci. 30 (2008), https://doi.org/10.1111/j.1468-2494.2008.00433.x.

[27] S.A. Fereig, G.M. El-Zaafarany, M.G. Arafa, M.M.A. AbdelMottaleb, Tackling the various classes of nano-therapeutics employed in topical therapy of psoriasis, Drug Deliv. 27 (1) (2020), https://doi.org/10.1080/10717544.2020.1754527.

[28] L.H. Higa, et al., Bacterioruberin from Haloarchaea plus dexamethasone in ultra-small macrophage-targeted nanoparticles as potential intestinal repairing agent, Colloids Surf., B 191 (2020), https://doi.org/10.1016/j.colsurfb.2020.110961.

[29] M. De Lourdes Moreno, C. Sánchez-Porro, M.T. García, E. Mellado, Carotenoids' production from halophilic bacteria, Methods Mol. Biol. 892 (2012), https://doi.org/10.1007/978-1-61779-879-5_12.

[30] M.J. Altube, S.M. Selzer, M.A. De Farias, R.V. Portugal, M.J. Morilla, E.L. Romero, Surviving nebulization-induced stress: dexamethasone in pH-sensitive archaeosomes, Nanomedicine 11 (16) (2016), https://doi.org/10.2217/nnm-2016-0165.
[31] M. Kates, S.C. Kushwaha, Archaea: A Laboratory Manual, 1995. Halophiles.
[32] C.J.F. Böttcher, C.M. Van gent, C. Pries, A rapid and sensitive sub-micro phosphorus determination, Anal. Chim. Acta 24 (1961), https://doi.org/10.1016/0003-2670(61)80041-X.
[33] L.H. Higa, et al., Ultradeformable archaeosomes as new topical adjuvants, Nanomed. Nanotechnol. Biol. Med. 8 (8) (2012), https://doi.org/10.1016/j.nano.2012.02.008.
[34] Z. Šesták, G. Britton, S. Liaaen-Jensen, H. Pfander (Eds.), Carotenoids. Handbook," Photosynthetica, vol. 42, 2004, https://doi.org/10.1023/b:phot.0000040641.40049.19, 2.
[35] L.H. Higa, H. Jerez, M.A. de Farias, R.V. Portugal, E.L. Romero, M.J. Morilla, Ultra-small, highly negatively charged archaeolipid nanoparticles for active targeting to macrophages of the inflamed mucosa, Nanomedicine 12 (10) (2017), https://doi.org/10.2217/nnm-2016-0437.
[36] A. Rahman, M.M. Rahman, M.S. Hossain, M.S. Jahan, N.J. Akter, M.L. Bari, A simple and alternative UV spectrometric method for the estimation of Vitamin D3, Microbial Bioactives 2 (1) (2019), https://doi.org/10.25163/microbbioacts.212086A2127261219.
[37] K.T. Plajnšek, S. Pajk, B. Govedarica, S. Pečar, S. Srčič, J. Kristl, A novel fluorescent probe for more effective monitoring of nanosized drug delivery systems within the cells, Int. J. Pharm. 416 (2011), https://doi.org/10.1016/j.ijpharm.2011.06.046.
[38] V. Teeranachaideekul, P. Boonme, E.B. Souto, R.H. Müller, V.B. Junyaprasert, Influence of oil content on physicochemical properties and skin distribution of Nile red-loaded NLC, J. Contr. Release 128 (2008), https://doi.org/10.1016/j.jconrel.2008.02.011.
[39] J.Y. Fang, C.L. Fang, C.H. Liu, Y.H. Su, Lipid nanoparticles as vehicles for topical psoralen delivery: solid lipid nanoparticles (SLN) versus nanostructured lipid carriers (NLC), Eur. J. Pharm. Biopharm. 70 (2) (2008), https://doi.org/10.1016/j.ejpb.2008.05.008.
[40] Ž. Temova, R. Roškar, Stability-indicating HPLC-UV method for Vitamin D3 determination in solutions, nutritional supplements and pharmaceuticals, J. Chromatogr. Sci. 54 (2016), https://doi.org/10.1093/chromsci/bmw048.
[41] T. Mosmann, Rapid colorimetric assay for cellular growth and survival: application to proliferation and cytotoxicity assays, J. Immunol. Methods 65 (1983), https://doi.org/10.1016/0022-1759(83)90303-4.
[42] B. Mishra, G. Wang, Individual and combined effects of engineered peptides and antibiotics on *Pseudomonas aeruginosa* biofilms, Pharmaceuticals 10 (3) (2017), https://doi.org/10.3390/ph10030058.
[43] L. Battaglia, E. Ugazio, Lipid nano- and microparticles: an overview of patent-related research, J. Nanomater. (2019), https://doi.org/10.1155/2019/2834941.
[44] G.S.M. Borges, et al., Sclareol is a potent enhancer of doxorubicin: evaluation of the free combination and co-loaded nanostructured lipid carriers against breast cancer, Life Sci. 232 (2019), https://doi.org/10.1016/j.lfs.2019.116678.
[45] E.B. Lages, et al., Co-delivery of doxorubicin, docosahexaenoic acid, and α-tocopherol succinate by nanostructured lipid carriers has a synergistic effect to enhance antitumor activity and reduce toxicity, Biomed. Pharmacother. 132 (2020), https://doi.org/10.1016/j.biopha.2020.110876.
[46] K. Jores, A. Haberland, S. Wartewig, K. Mäder, W. Mehnert, Solid Lipid Nanoparticles (SLN) and oil-loaded SLN studied by spectrofluorometry and Raman spectroscopy, Pharm. Res. (N. Y.) 22 (11) (2005), https://doi.org/10.1007/s11095-005-7148-5.
[47] A. Saupe, K.C. Gordon, T. Rades, Structural investigations on nanoemulsions, solid lipid nanoparticles and nanostructured lipid carriers by cryo-field emission scanning electron microscopy and Raman spectroscopy, Int. J. Pharm. 314 (1) (2006), https://doi.org/10.1016/j.ijpharm.2006.01.022.
[48] N. Ahmad, M. Saleem, Raman spectroscopy based characterization of desi ghee obtained from buffalo and cow milk, Int. Dairy J. 89 (2019), https://doi.org/10.1016/j.idairyj.2018.08.013.
[49] S.P. Cannavo, F. Guarneri, R. Giuffrida, E. Aragona, C. Guarneri, Evaluation of cutaneous surface parameters in psoriatic patients, Skin Res. Technol. 23 (2017), https://doi.org/10.1111/srt.12299.
[50] T. Ramezanli, B.E. Kilfoyle, Z. Zhang, B.B. Michniak-Kohn, Polymeric nanospheres for topical delivery of vitamin D3, Int. J. Pharm. 516 (1–2) (2017), https://doi.org/10.1016/j.ijpharm.2016.10.072.
[51] E. Glowka, J. Stasiak, J. Lulek, Drug delivery systems for vitamin D supplementation and therapy, Pharmaceutics 11 (7) (2019), https://doi.org/10.3390/pharmaceutics11070347.
[52] Y.M. Hemery, et al., Influence of light exposure and oxidative status on the stability of vitamins A and D3 during the storage of fortified soybean oil, Food Chem. 184 (2015), https://doi.org/10.1016/j.foodchem.2015.03.096.
[53] M.J. Altube, L.I. Caimi, C. Huck-Iriart, M.J. Morilla, E.L. Romero, Reparation of an inflamed air-liquid interface cultured a549 cells with nebulized nanocurcumin, Pharmaceutics 13 (9) (2021), https://doi.org/10.3390/pharmaceutics13091331.
[54] F. Mandelli, V.S. Miranda, E. Rodrigues, A.Z. Mercadante, Identification of carotenoids with high antioxidant capacity produced by extremophile microorganisms, World J. Microbiol. Biotechnol. 28 (4) (2012), https://doi.org/10.1007/s11274-011-0993-y.
[55] G. Squillaci, R. Parrella, V. Carbone, P. Minasi, F. La Cara, A. Morana, Carotenoids from the extreme halophilic archaeon Haloterrigena turkmenica: identification and antioxidant activity, Extremophiles 21 (5) (2017), https://doi.org/10.1007/s00792-017-0954-y.
[56] J. Hou, H.L. Cui, *Vitro* antioxidant, antihemolytic, and anticancer activity of the carotenoids from Halophilic Archaea, Curr. Microbiol. 75 (3) (2018), https://doi.org/10.1007/s00284-017-1374-z.
[57] A. Fariq, A. Yasmin, M. Jamil, Production, characterization and antimicrobial activities of bio-pigments by Aquisalibacillus elongatus MB592, Salinicoccus sesuvii MB597, and Halomonas aquamarina MB598 isolated from Khewra Salt Range, Pakistan, Extremophiles 23 (2019), https://doi.org/10.1007/s00792-019-01095-7.
[58] K. Sahli, M.A. Gomri, J. Esclapez, P. Gómez-Villegas, O. Ghennai, M.J. Bonete, R. León, K. Kharroub, Bioprospecting and characterization of pigmented halophilic archaeal strains from Algerian hypersaline environments with analysis of carotenoids produced by *Halorubrum sp*. BS2, J. Basic Microbiol. 60 (7) (2020), https://doi.org/10.1002/jobm.202000083.
[59] P. Gómez-villegas, J. Vigara, M. Vila, J. Varela, L. Barreira, R. Léon, Antioxidant, antimicrobial, and bioactive potential of two new haloarchaeal strains isolated from Odiel salterns (Southwest Spain), Biology 9 (9) (2020), https://doi.org/10.3390/biology9090298.
[60] G.E. Hegazy, M.M. Abu-Serie, G.M. Abo-Elela, H. Ghozlan, S.A. Sabry, N. A. Soliman, Y.R. Abdel-Fattah, *In vitro* dual (anticancer and antiviral) activity of the carotenoids produced by haloalkaliphilic archaeon Natrialba sp. M6, *Sci. Rep*. 10 (2020), https://doi.org/10.1038/s41598-020-62663-y.
[61] L. Zalazar, et al., Bacterioruberin extracts from a genetically modified hyperpigmented Haloferax volcanii strain: antioxidant activity and bioactive properties on sperm cells, J. Appl. Microbiol. 126 (2019), https://doi.org/10.1111/jam.14160.
[62] C. Lizama, et al., Analysis of carotenoids in Haloarchaea species from Atacama Saline lakes by High Resolution UHPLC-Q-Orbitrap-Mass Spectrometry: antioxidant potential and biological effect on cell viability, Antioxidants 10 (2021), https://doi.org/10.3390/antiox10081230.
[63] H.R. Shahmohammadi, et al., Protective roles of bacterioruberin and intracellular KCl in the resistance of Halobacterium salinarium against DNA-damaging Agents, J. Radiat. Res. 39 (2008) 251–262, https://doi.org/10.1269/jrr.39.251.
[64] K. Pfeifer, I. Ergal, M. Koller, M. Basen, B. Schuster, S.K.-M.R. Rittmann, Archaea biotechnology, Biotechnol. Adv. 47 (2021), https://doi.org/10.1016/j.biotechadv.2020.107668.
[65] S.A. Wissing, A. Lippacher, R.H. Müller, Investigations on the occlusive properties of solid lipid nanoparticles (SLN), J. Cosmet. Sci. 52 (5) (2001).
[66] B. Flutter, F.O. Nestle, TLRs to cytokines: mechanistic insights from the imiquimod mouse model of psoriasis, Eur. J. Immunol. 43 (12) (2013), https://doi.org/10.1002/eji.201343801.
[67] J.A. Deane, S. Bolland, Nucleic acid-sensing TLRs as modifiers of autoimmunity, J. Immunol. 177 (10) (2006), https://doi.org/10.4049/jimmunol.177.10.6573.
[68] J. Fuentes-Duculan, et al., A subpopulation of CD163-positive macrophages is classically activated in psoriasis, J. Invest. Dermatol. 130 (2010) 10, https://doi.org/10.1038/jid.2010.165.
[69] R.A. Clark, T.S. Kupper, Misbehaving macrophages in the pathogenesis of psoriasis, J. Clin. Investig. 116 (2006) 8, https://doi.org/10.1172/JCI29441.
[70] R. Lai, D. Xian, X. Xiong, L. Yang, J. Song, J. Zhong, Proanthocyanidins: novel treatment for psoriasis that reduces oxidative stress and modulates Th17 and Treg cells, Redox Rep. 23 (2018) 1, https://doi.org/10.1080/13510002.2018.1462027.
[71] G. Arango Duque, A. Descoteaux, Macrophage cytokines: involvement in immunity and infectious diseases, Front. Immunol. 5 (2014), https://doi.org/10.3389/fimmu.2014.00491.
[72] X. Yu, et al., Pattern recognition scavenger receptor CD204 attenuates toll-like receptor 4-induced NF-κB activation by directly inhibiting ubiquitination of Tumor Necrosis Factor (TNF) receptor-associated factor 6, J. Biol. Chem. 286 (21) (2011), https://doi.org/10.1074/jbc.M111.224345.
[73] H. Yi, et al., Pattern recognition scavenger receptor SRA/CD204 down-regulates Toll-like receptor 4 signaling-dependent CD8 T-cell activation, Blood 113 (23) (2009), https://doi.org/10.1182/blood-2008-11-190033.
[74] L. Skov, et al., IL-8 as antibody therapeutic target in inflammatory diseases: reduction of clinical activity in palmoplantar pustulosis, J. Immunol. 181 (1) (2008), https://doi.org/10.4049/jimmunol.181.1.669.
[75] C.Y. Ng, Y.H. Huang, C.F. Chu, T.C. Wu, S.H. Liu, Risks for Staphylococcus aureus colonization in patients with psoriasis: a systematic review and meta-analysis, Br. J. Dermatol. 177 (4) (2017), https://doi.org/10.1111/bjd.15366.
[76] D.T. Masallat, W. Eldars, A.F. State, D. Moemen, Panton-Valentine leukocidin-positive methicillin-resistant Staphylococcus aureus correlates with disease severity in psoriasis: a case–control study, Egyp. J. Basic Appl. Sci. 6 (1) (2019), https://doi.org/10.1080/2314808x.2019.1681662.
[77] H.W. Chang, et al., Alteration of the cutaneous microbiome in psoriasis and potential role in Th17 polarization, Microbiome 6 (1) (2018), https://doi.org/10.1186/s40168-018-0533-1.
[78] S. Saputo, R.C. Faustoferri, R.G. Quivey, Vitamin D compounds are bactericidal against Streptococcus mutans and target the bacitracin-associated efflux system, Antimicrob. Agents Chemother. 62 (1) (2018), https://doi.org/10.1128/aac.01675-17.
[79] A.P. Perez, et al., The anti MRSA biofilm activity of Thymus vulgaris essential oil in nanovesicles, Phytomedicine 57 (2019), https://doi.org/10.1016/j.phymed.2018.12.025.
[80] K. Sahli, et al., Bioprospecting and characterization of pigmented halophilic archaeal strains from Algerian hypersaline environments with analysis of

carotenoids produced by *Halorubrum* sp. BS2, J. Basic Microbiol. 60 (7) (2020), https://doi.org/10.1002/jobm.202000083.

[81] P. Gómez-villegas, J. Vigara, M. Vila, J. Varela, L. Barreira, R. Léon, Antioxidant, antimicrobial, and bioactive potential of two new haloarchaeal strains isolated from odiel salterns (Southwest Spain), Biology 9 (9) (2020), https://doi.org/10.3390/biology9090298.

[82] R.H. Müller, R.D. Petersen, A. Hommoss, J. Pardeike, Nanostructured lipid carriers (NLC) in cosmetic dermal products, Adv. Drug Deliv. Rev. 59 (6) (2007), https://doi.org/10.1016/j.addr.2007.04.012.